Soft Matter

PERSPECTIVE

View Article Online
View Journal | View Issue

Cite this: *Soft Matter*, 2018, **14**, 2961

Received 5th January 2018,
Accepted 21st February 2018

DOI: 10.1039/c8sm00044a

rsc.li/soft-matter-journal

Dynamics of associative polymers

Zhijie Zhang,[a] Quan Chen*[a] and Ralph H. Colby[b]

Current progress in understanding the dynamics of associating polymers is reviewed, with examples including both ionic and hydrogen bonding associations. A particular emphasis is placed on quantification of the strength of the interaction that sets the association lifetime. Knowledge of the interaction energy and the number density of associating groups allows a rational understanding of the linear viscoelastic response of many associating polymers.

I. Introduction

Introduction of inter-chain interactions into polymers modifies their dynamics. For example, introduction of covalent bonds among linear polymer chains would result in a chemical sol or gel.[1] Introduction of weaker attractive interactions, like ionic, hydrogen bonding, hydrophobic, or π–π stacking (see Fig. 1), would result in a physical sol/gel. The different dynamic behavior stems from different lifetimes, densities and positions of the associative (interactive) sites of the chain.

Lifetime is usually controlled by interaction energy. Fig. 2 compares the energy for the covalent bond and several physical interactions. $kT = 2.5$ kJ mol^{-1} is the thermal energy at ambient temperature and pressure. The energy of a covalent bond is usually $>100\times$ larger than the thermal energy, and thus the chemical sol or gel based on covalent bonds is stable at ambient temperatures and pressures. In comparison, the ionic, hydrogen bonding, or van der Waals interactions are usually closer to (one order higher than or at the same order of) the thermal energy.[2,3] Therefore, the formation and breakup of these interactions could enter the time scale of our observation, and thus become reversible. (van der Waals interactions weaker

[a] State Key Laboratory of Polymer Physics and Chemistry, Changchun Institute of Applied Chemistry, Chinese Academy of Sciences, Changchun 130022, China. E-mail: qchen@ciac.ac.cn
[b] Department of Materials Science and Engineering, The Pennsylvania State University, University Park, PA 16802, USA

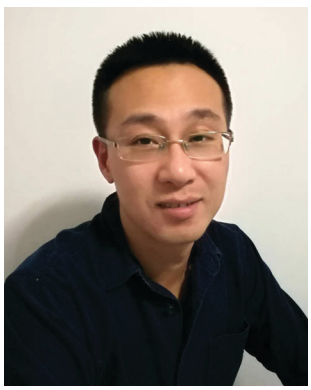

Zhijie Zhang

Zhijie Zhang received his BS in 2001, MS in 2005, and PhD in 2008 from Jilin University. His PhD research was on phase separation of binary distributed high-density polyethylene. He began working as a research assistant at the Changchun Institute of Applied Chemistry, Chinese Academy of Sciences in 2008, and was promoted to an associate professor in 2017. His current research interest is the dynamics of various polymer-related systems, using state-of-the-art rheological and dielectric techniques.

Quan Chen

Quan Chen received his BS and MS in the School of Chemistry and Chemical Engineering from Shanghai Jiaotong University in 2003 and 2007, respectively, and PhD degree in the Graduate School of Engineering, Kyoto University, Japan in 2011 working on dynamics of miscible polymer blends with Prof. Hiroshi Watanabe. He began working as a postdoc at the Pennsylvania State University with Prof. Ralph Colby on designing single-ion conductors in 2012, and moved to his current position as a Professor at the Changchun Institute of Applied Chemistry, Chinese Academy of Sciences in 2015. His current research interests are molecular rheology of polymer-related systems.

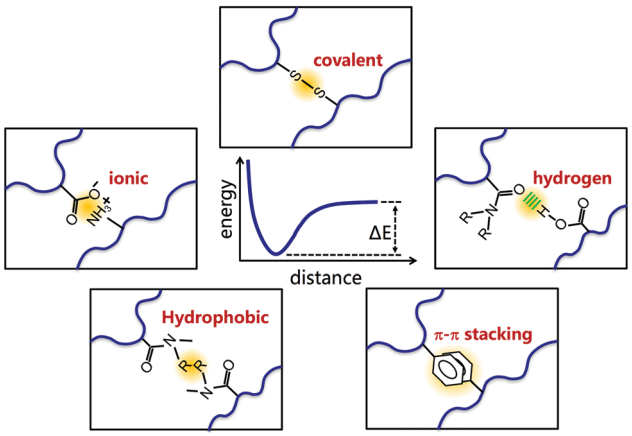

Fig. 1 Schematic illustration of the chemical covalent bond, and physical interactions including ionic bonding, hydrogen bonding, hydrophobic interactions (in water with R = alkyl) and π−π stacking.

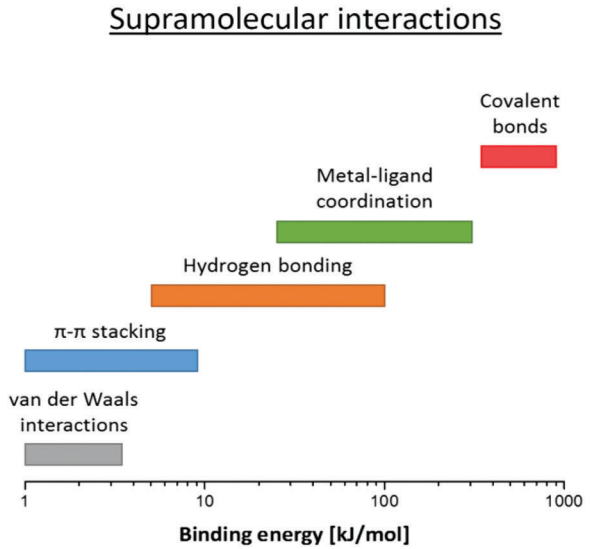

Fig. 2 Energy ranges of different types of interactions. Reprinted with the permission of the Society of Rheology from van Ruymbeke.[7]

than kT would only result in a subtle enhancement of 'ordinary' friction in the liquid state.) The reversibility is critical to realize functions of novel materials including self-healing, stimuli-responsive, and shape memory materials,[4,5] and more importantly, to realize physiological mechanisms of many biopolymers. For example, both the folding and unfolding of the protein, and the winding and unwinding of DNA chains rely on the reversibility of the intra- or inter-chain interactions.[6]

The number density of the interactions is also very important. The traditional classification of ion-containing polymers is based on their ion content. For example, polymers that have a small fraction of ionic monomers, usually less than 10%, are classified as ionomers.[8,9] The ionomers are usually processable and usable in bulk. In contrast, polyelectrolytes usually have a higher fraction of ionic groups (~100%), endowing them with both the electrolyte (salt) and polymer properties. Due to the high fraction of ions and strong ionic aggregation, polyelectrolytes are usually non-processable in bulk and are applied in solutions.[1,10] The counterion can partly or completely dissociate in solution, depending on the strength and spacing of the ionic groups and the polarity of the solvent. Counterion dissociation leaves the polyelectrolyte chain with a net charge, giving it an extended conformation.[11,12] Such ionic dissolution can lead to an increase of the reduced viscosity with dilution, known as the "polyelectrolyte effect".[12]

Obviously, the dynamics should depend on the lifetime, density and position of the associative sites of the chain. And the interaction could be either "attractive" or "repulsive", depending on the interaction group and polarity of its medium. This review placed a main focus on those random associative polymers where the "attractive" interactions prevail and have a random distribution. For the ion-containing systems, we first attempt to specify a boundary between the ionomer and polyelectrolyte through considering both the density and strength of the ionic interactions.[13,14] After that, we explain how the dynamics of strongly associative polymers, including ionomers and hydrogen bonding polymers, are controlled by the density of the associative groups, *i.e.* the stickers. The focus is placed on two important transitions, a sol-to-gel transition occurring at approximately one effective interchain sticker per chain for associating polymers,[15,16] and a single to double plateau transition occurring at approximately one effective interchain sticker per entanglement for entangled associating polymers.[17,18] Finally, we explain the experimental determination of the association energy.[16,19]

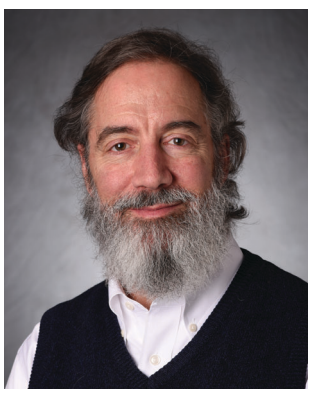

Ralph H. Colby

Ralph H. Colby received his BS in Materials Science and Engineering from Cornell University in 1979 and his MS and PhD in Chemical Engineering from Northwestern University, in 1983 and 1985. After ten years at the Eastman Kodak Company in their Corporate Research Laboratories, Dr Colby joined the faculty in Materials Science and Engineering at the Pennsylvania State University in 1995. He is the current Editor of the Journal of Rheology and was the recipient of the Society of Rheology's Bingham Medal in 2012. Dr Colby has over 200 publications and published a textbook Polymer Physics in 2003.

II. Ionomers and polyelectrolytes, a molecular view

As explained earlier, ionomers and polyelectrolytes are traditionally defined from their ion content. The definition faces a problem for certain samples that behave as ionomers in low polarity solvents, but as polyelectrolytes in polar solvents.[20–27]

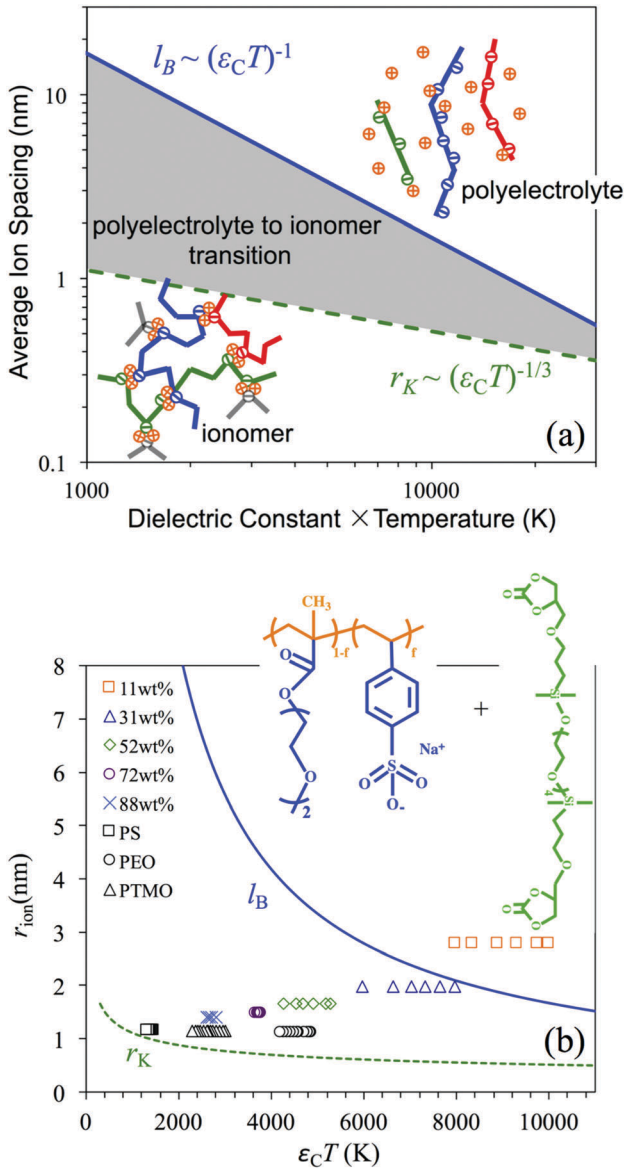

Fig. 3 Comparison of the average distance between ions, r_{ion}, the Bjerrum length, l_B, and the Keesom length, r_K based on the ion pair dipole of sodium sulfonate, μ = 15.2 Debye. (a) These lengths are plotted against the product of dielectric constant ε_C and absolute temperature T on logarithmic scales. (b) The colorful symbols are r_{ion} plotted against $\varepsilon_C T$ on linear scales, for mixtures of an ionomer and a polar plasticizer with the content of the ionomer as indicated. The inset shows the chemical structures of the ionomer and plasticizer. The black symbols are ionomers with attached sulfonate groups and sodium as the counterion, based on polystyrene, poly(ethylene oxide), and poly(tetramethylene oxide).

Eisenberg and coworkers realized the problem and provided definitions based on the status of ionic groups: ionomers are "polymers in which bulk properties are governed by ionic interactions in discrete regions (ionic aggregation)", whereas polyelectrolytes are "polymers in which solution properties in solvents of high dielectric constants are governed by electronic static interactions over distances larger than typical molecular dimensions".[8,9]

This definition is stricter than the definition simply based on the ion content. Nevertheless, it is based on the structure rather than the thermodynamics that leads to the structure. The aggregation status should be related to a competition between the thermal energy kT that dissociates the ions and the electrostatic energy that favors the association, $\sim e^2/\varepsilon\varepsilon_0 r$, where e is the unit charge, ε and ε_0 are the dielectric constant and the permittivity of vacuum, respectively, and r is an average distance between charges.[2] The polyelectrolyte regime should correspond to the case where:[3]

$$\frac{e^2}{\varepsilon\varepsilon_0 r} \ll kT \quad (1)$$

allowing r to be large. The ionomer instead has:[3]

$$\frac{e^2}{\varepsilon\varepsilon_0 r} \gg kT \quad (2)$$

forcing r to remain small. This definition leaves an unclear crossover zone where the ions are partially associated. We recently defined a boundary of the crossover zone through considering both the strength and density of the interactions, as shown in Fig. 3(a).[14] The vertical axis, r_{ion}, is the average distance between neighboring ions, and the horizontal axis, the product of dielectric constant and temperature εT, characterizes the polarity of the medium. The blue solid line is the well-known Bjerrum length,

$$l_B \equiv e^2/(4\pi\varepsilon_C\varepsilon_0 kT) \quad (3)$$

a distance between elementary charges e where the magnitude of the Coulomb energy (between charges) equals the thermal energy, with $l_B \sim (\varepsilon T)^{-1}$. The green dashed line is a newly defined Keesom length,[13,14]

$$r_K = \left[\mu^2 \Big/ \left(2\sqrt{6}\pi\varepsilon_C\varepsilon_0 kT\right)\right]^{1/3} \quad (4)$$

a distance between ion pair dipoles with dipole moment μ, where the Keesom energy (between ionic dipoles) is equal to the thermal energy, with $r_K \sim (\varepsilon T)^{-1/3}$. Here, ε_C is a relevant dielectric constant for motion of ions or dipoles, as explained later in more detail. The two lines divide the diagram in Fig. 3 into three regimes, a polyelectrolyte regime above the solid blue line, an ionomer regime below the dashed green line, and a transition regime in between the two lines.

For $r_{ion} \geq l_B$ the material is a polyelectrolyte with many dissociated ions and no ion aggregates. For $r_{ion} \leq r_K$ the material is an ionomer with no dissociated counterions and most ions in ionic aggregates. For $r_K < r_{ion} < l_B$ there is a gradual transition between the ionomer and the polyelectrolyte that has the character of both,[13,14] with ion aggregates, isolated ion pairs and dissociated ions in equilibrium. There is a natural dissociation parameter that allows quantification of the extent of dissociation (and aggregation) although the details of how this parameter is connected to extents of dissociation and aggregation are still a subject of active research.

$$\Phi \equiv \frac{r_{ion} - r_K}{l_B - r_K} \quad (5)$$

$\Phi \leq 0$ ($r_{ion} \leq r_K$) is the clean ionomer limit with no dissociated counterions and most ions in ion aggregates, while $\Phi \geq 1$ ($r_{ion} \geq l_B$)

is the polyelectrolyte limit with many dissociated counterions and no ion aggregates. The sodium salt of sulfonated polystyrene in water at room temperature has $\varepsilon_C T = 23\,000$ K and hence cannot be put onto the linear scales of Fig. 3(b) but is deep into the polyelectrolyte regime.

Fig. 3(b) compares l_B (solid blue curve), r_K (dashed green curve) and r_{ion} (symbols) plotted against $\varepsilon_C T$ on linear scales. For those ion-containing polymers, the polarity of the medium is characterized using dielectric spectroscopy. For the ionomer/plasticizer mixtures, the dielectric spectroscopy detected three processes: (1) an α-relaxation of the EO segments, (2) a slower α_2-process where the ions in aggregates, ion pairs and isolated ions all exchange states, and (3) and an electrode polarization process corresponding to the polarization of ions at the two electrodes.[13] (An example with data is given later in Fig. 8(b).) The characteristic dielectric constant for the dipole fluctuation, ε_C, is chosen to be the effective dielectric constant for ionic interactions, after the α-relaxation while before the α_2-process. In contrast, much of the ionomer literature, including those from our own groups, focuses on the larger static dielectric constant evaluated after the α_2-process rearranges the ions.

The colorful symbols in Fig. 3(b) show r_{ion} against $\varepsilon_C T$ of a model system, *i.e.* mixtures of a poly(ethylene oxide) (PEO) based ionomer and an EO-based polar plasticizer, with chemical structures shown in the inset.[13,14] The EO units (of both the ionomer and the plasticizer) can soften the electrostatic interaction between ions, and the cyclic carbonate end groups (of the plasticizer) can effectively enhance the dielectric constant, both enabling a crossover zone to be well observed by changing the plasticizer content. Two trends are revealed through increasing the plasticizer content (decreasing the ionomer content from 88 wt% to 11 wt%, as indicated), *i.e.* an increase of the average distance between ions, r_{ion}, and an enhancement of the polarity of the medium, $\varepsilon_C T$. Finally, the 11 wt% sample enters the polyelectrolyte regime, with $r_{ion} > l_B$ and $\Phi > 1$ for the sample with 11 wt% ionomer.

For comparison, the black symbols in Fig. 3(b) show r_{ion} against $\varepsilon_C T$ of three ionomers, with PS (with 9.5 mol% of styrene monomers sulfonated[28]), PEO (with poly(ethylene oxide) of M = 600 between sulfonated phthalates[29,30]), and PTMO (with poly(tetramethylene oxide) of M = 650 between sulfonated phthalates[30,31]) as backbones, the sulfonate group as the attached anion, and sodium as the counterion. The PEO and PTMO samples were synthesized by condensation polymerization from PTMO and PEO diols and sulfonated isophthalate diester. The diols are nearly monodisperse ($M_w/M_n < 1.1$), making the stickers uniformly distributed along the PEO and PTMO ionomer chains.

Since the ionic groups are the same for all the samples shown in Fig. 3(b), the Keesom length r_K is the same for these three samples (green curve). We found that the three ionomer samples and the 88 wt% sample have r_{ion} close to r_K ($\Phi < 0.2$) just outside the ionomer regime defined by r_K. For these samples we hence expect very few dissociated ions and considerable ion aggregation, with some ion pairs present. For the PS ionomers (black squares) $\Phi < 0.05$ and nearly all ions are in ion aggregates;[28] the conductivity is very small (suggesting no dissociated ions) and the static (low frequency) dielectric constant is also very small above T_g, suggesting very few isolated ion pairs that can respond to the applied field. The PEO ionomer aggregates ions on heating[29] (higher T means smaller $\varepsilon_C T$ for the PEO ionomer in Fig. 3(b)) and an electrode polarization analysis suggests only a tiny fraction of $\sim 10^{-3}$ of sodium ions are in a conducting state near room temperature,[30] while the PTMO ionomer with $\Phi < 0.1$ has even smaller fraction of $\sim 10^{-6}$ of sodium ions in the conducting state near room temperature.[30]

The morphological changes for the mixtures of ionomer and plasticizer during this ionomer-to-polyelectrolyte transition are shown in the form of X-ray scattering data in Fig. 4(a),[14,32–34] where the high q, medium q and low q local maxima of the ionomer sample (100 wt%) correspond to amorphous halo, correlation of interchain spacing, and spacing between ion aggregates, respectively. The dissolution of the ionomer significantly reduces the amplitude of the ionic peak, and finally the 11 wt% sample shows a scattering pattern similar to that of the plasticizer (0 wt%), meaning that the ionic groups are almost completely dissociated, consistent with the polyelectrolyte regime. Fig. 4(b) compares the scattering profiles of the pure ionomers that were included earlier in Fig. 3(b). All materials in Fig. 3 and 4 have sulfonate as the attached anion and sodium as the counterion, and the ion content is very similar for these samples, so that the distance r_{ion} is nearly the same in Fig. 3(b). Changing the polymer backbone has a remarkable effect on the degree of aggregation because this changes ε_C and hence Φ. The PEO based ionomer shows that ion aggregation intensifies with increasing temperature, due to a decrease of polarity of the medium.[29] Even at the highest temperature (T = 120 °C), the PEO based ionomer having EO in the backbone exhibits a weaker ion aggregation peak than the 100 wt% sample having EO as side chains. The two ionomers having EO units, either in the backbone or in side chains, show much weaker ionic aggregation than the PTMO and PS based ionomers, due to the well-known ion solvation ability of PEO, which can coordinate with ionic groups to reduce their aggregation energy by forming separated ion pairs that enhance the dielectric constant.

The dynamic change along with the ionomer to polyelectrolyte transition is shown in Fig. 4(c), where pseudo LVE master curves of storage and loss moduli, G' and G'', are compared. (The time temperature superposition works reasonably at low temperatures where the association remains almost intact and at high temperature where the dissociation occurs frequently, but not at intermediate temperatures.)[15] The 100 wt% sample shows a clear plateau at low frequency, an indication of physical gelation, while the 11 wt% sample flows after the glass transition of the solvent (as shown in black symbols). The transition from 100 wt% to 11 wt% is remarkable: first, a narrowing of the glassy modulus ($\gg 10^6$ Pa) is seen, which is well expected from the classic Eisenberg restricted zone model (see the inset):[8,28,36–38] the motion of polymer segments within a Kuhn length of the ionic aggregate (in the orange region) is strongly restricted, enabling them to exhibit T_g higher than

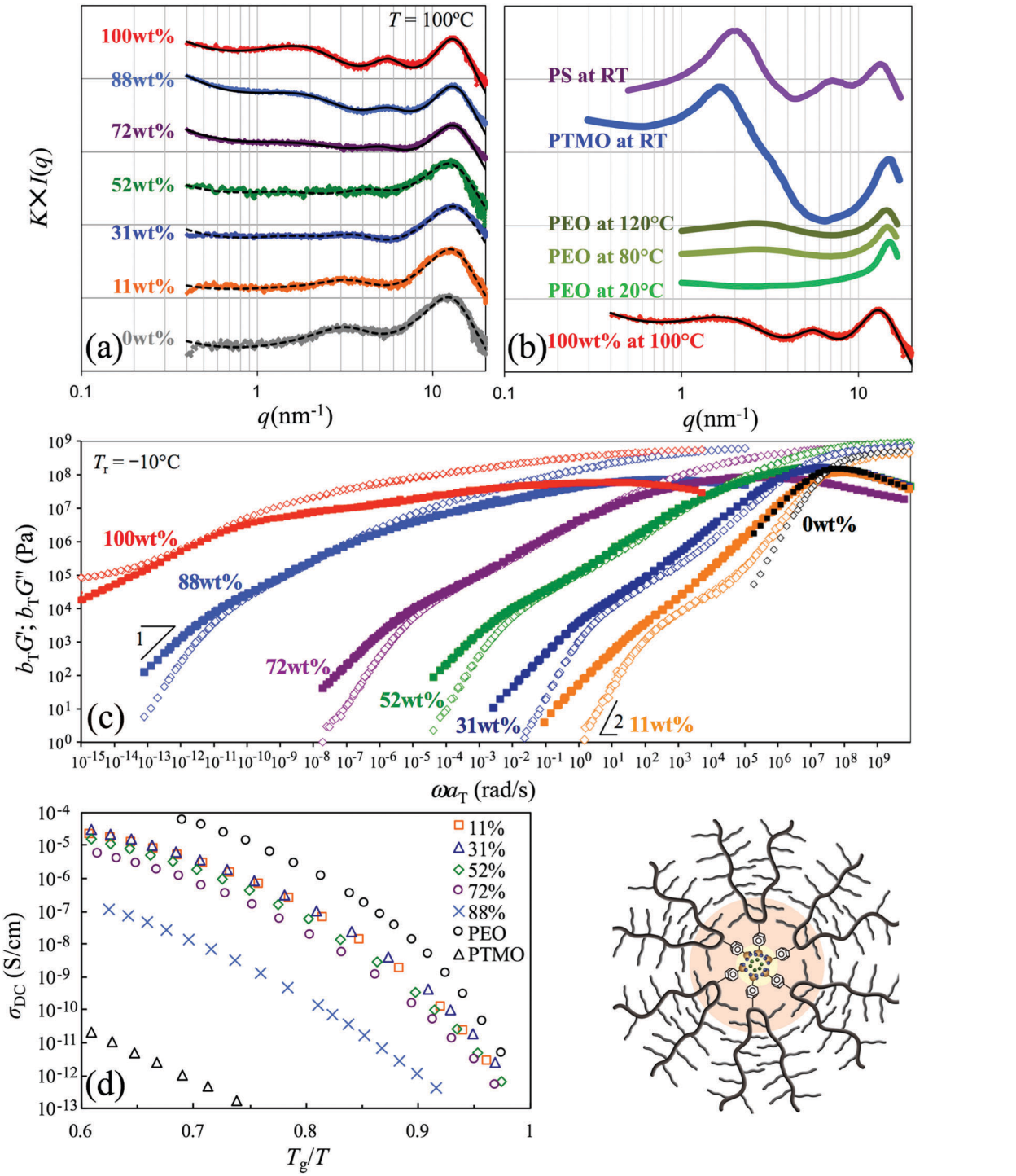

Fig. 4 Comparison of the X-ray scattering profile[14] of (a) the ionomer (100 wt%), ionomer/plasticizer mixtures (88–11 wt%), and the plasticizer (0 wt%) and (b) the ionomer (100 wt%) and ionomers based on PEO, PTMO, and PS backbones. (c) Pseudo LVE master curves[15] of the ionomer (100 wt%), ionomer/plasticizer mixtures (88–11 wt%), and plasticizer (0 wt%) shown as black symbols, and (d) DC conductivity σ_{DC} plotted against T_g/T. The inset is a schematic illustration of the classic Eisenberg restricted zone model.[8,36] The regions in yellow, orange, and white correspond to ion aggregation, restricted region (where the segmental mobility is restricted by the ion aggregation), and non-restricted region (where the segments far away from the ion aggregates are not restricted), respectively.[35]

segments far away from the ion aggregates (in the white region). The glass transition process broadens greatly as the ionomer content is increased because monomers find themselves in a broad distribution of the surrounding polymeric segments (*i.e.*, various numbers of restricted monomers within a Kuhn length of a given monomer). Second, the terminal relaxation

accelerates as plasticizer is added. This acceleration is much stronger than just the T_g change, because the distribution of the rubbery modulus ($<10^6$ Pa) narrows significantly. Detailed analysis shows that the acceleration of terminal relaxation, accompanied by a narrowing of the relaxation time distribution, is due to a combination effect of plasticizing (lowering T_g) and softening of ionic interactions with an increasing fraction of the polar solvent.[13]

The ionic conductivity σ_{DC} in Fig. 4(d) is also strongly related to the ionomer-to-polyelectrolyte transition, which leads to more dissociated ions and thus promotes ionic conductivity. The only exception is the PEO ionomer with $\Phi < 0.2$ but exhibits σ_{DC} even higher than the 11% solution with $\Phi > 1$, within the polyelectrolyte regime. This feature should be related to the well-known ion-solvating ability of the PEO backbone, which enables the PEO ionomer to be a superior polymer electrolyte. The vital underlying reason is that the PEO ionomer has segments with 13 ethylene oxide repeats that allow the formation of separated ion pairs with larger dipoles (Fig. 3 only used the dipoles of contact ion pairs to calculate the Keesom length) reflected in the static (low frequency) dielectric constant near room temperature ($\sim$35 for the 11% solution[13] *vs.* $\sim$100 for the PEO ionomer[31]). This separated pair hypothesis explains much of the 'magic' of PEO as a polymer electrolyte, as the dipole of the ethylene oxide repeat is quite small (1 Debye) and its room temperature dielectric constant is only 7, yet alkali salts dissolve in PEO with high conductivity.[39,40] Small cations such as Li or Na prefer to be surrounded by four or five oxygens and a single PEO strand of sufficient length can supply all of those oxygens, owing to the flexibility of PEO that allows a structure surrounding the small cation similar to that of a crown ether. In contrast, FTIR proves that in the PEO ionomers, the benzene sulfonate–cation contact pair always prefers a monodentate structure (only one of the three sulfonate oxygens gets close to the cation).[41] The interaction between each of the close ether oxygens and the cation is about half of that with sulfonate. Collectively, this translates to a high proportion of ion pairs in a separated pair state with an ether oxygen between the cation and the sulfonate anion, as suggested by the observation that the static dielectric constant is higher than expected based on all ions being in an isolated contact pair state that can respond to the applied electric field. By forming separated ion pairs, PEO effectively gets the cation further from the anion, considerably lowering their interaction and facilitating ion transport. Simulations found that the cation can then 'hop' along the chain (the ether oxygen at one end of the wrapping strand is replaced by another at the other end).[42]

III. Density of stickers of associative polymers

When the ionic interaction is dominantly attractive, the ion-containing polymer shows a typical associative polymer behavior similar to those of hydrogen-bonding polymers or polymers containing incompatible groups (such as hydrophobic groups in a hydrophilic medium). Here the recent progress is summarized in understanding the effect of sticker density on chain dynamics.

3.1 Gelation

Most associating polymers have a small number fraction p of associating groups and many non-associating monomers with number fraction $1 - p$. For randomly placed associating groups along chains of N monomers, there is a gel point that is $p_c = 1/(N - 1)$, analogous to vulcanization (random chemical crosslinking) of long linear chains of N monomers,[1,43,44] because the effective functionality is N, meaning that each monomer has the same probability of being an associative monomer. With random placement of stickers, this gel point corresponds to an average of 1 associative group per chain.[15,43–45] Below the gel point ($p < p_c$) the associations only create branched species (the sol) while above the gel point ($p > p_c$) there is a gel that is in equilibrium with the sol. The degree of gelation can be defined by $\varepsilon = (p - p_c)/p_c$ such that $\varepsilon = -1$ (or $p = 0$) corresponds to no associative groups, $\varepsilon < 0$ is below the gel point, $\varepsilon = 0$ (or $p = p_c$) is the gel point, $0 < \varepsilon < 1$ is above the gel point with both sol and gel present and at $\varepsilon = 1$ (or $p = 2p_c$) almost all chains are attached to the gel, which has an average of 2 associative groups per chain. The molecular picture explained above has assumed that all the associating groups form effective associations, which is approximately valid for strong associative systems with association energy $E_a > 10kT$.

Linear chains of N monomers have $N^{1/2}$ other chains in their pervaded volume, and this overlapping of chains is described by an overlap parameter[1] $P = R^3/Nb^3 = N^{1/2}$ at $\varepsilon = -1$ (or $p = 0$), where $R = bN^{1/2}$ is the size of the precursor chains, making R^3 their pervaded volume. As associative groups are randomly placed on these chains, the growth in mass of sol chains in the mean field regime $N_{char}b^3 \sim |\varepsilon|^{-2}$ becomes faster than the growth in pervaded volume ${\xi_{char}}^3 \sim |\varepsilon|^{-3/2}$. More importantly, the size distribution of sol chains broadens as the gel point is approached, and the fraction of the sol that has the largest sol chain size $f \sim |\varepsilon|$ approaches 0 towards the gel point. These two changes lead to decreased $P \sim f{\xi_{char}}^3/N_{char} \sim |\varepsilon|^{3/2}$ of those sol chains as ε (<0) increases (see Fig. 5(a)).[1,15,46,47] At the Ginzburg point $-\varepsilon_G$ the overlap parameter reaches unity. For $-1 < \varepsilon < -\varepsilon_G$ there is significant overlap of branched sol chains and the mean-field Flory–Stockmayer theory applies, while closer to the gel point the overlap parameter remains at unity and the critical percolation theory applies ($-\varepsilon_G < \varepsilon < \varepsilon_G$). This overlap parameter is perfectly symmetric in the range $-1 < \varepsilon < 1$ (see Fig. 5a) meaning that for $\varepsilon_G < \varepsilon < 1$ the gel strands overlap to allow the mean field percolation theory to again apply. For $\varepsilon > 1$, the average strand size becomes smaller than that of the precursor chain, which contains $\sim\varepsilon$ strands, meaning that the number of monomers per strand, $N_{strand} \sim \varepsilon^{-1}$, and accordingly the overlapping of strands is $P \sim {N_{strand}}^{1/2} \sim \varepsilon^{-1/2}$.

With strong associations, the branched molecules in the sol relax as though the associations were permanent, following the Rouse model for the simplest case of the precursor chains being too short to have entanglements (the strong association

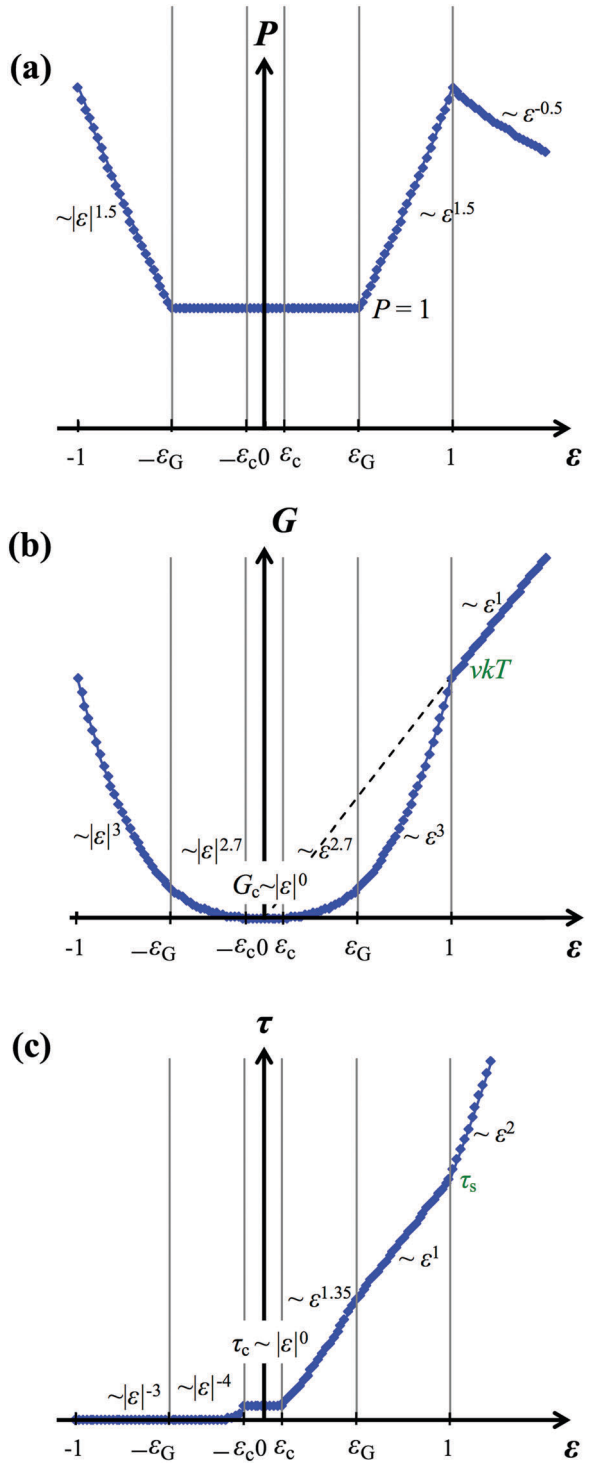

Fig. 5 Evolution of (a) the overlap parameter, (b) terminal relaxation modulus, and (c) terminal relaxation time, as functions of relative extent of sulfonation ε for unentangled associative polymers.

with $E_a > 10kT$ is the focus here. Dynamics of a weak associative system with the sticker lifetime ~ Rouse time was studied by Watanabe *et al.*[48–50]). A vital point is that if the precursor chains do not entangle, the larger randomly branched polymers closer to the gel point and the network strands beyond the gel point never have entanglement effects owing to hyperscaling.[1,51] The relaxation time τ increases as the gel point is approached from below and the terminal modulus G (kT per chain) decreases since more associations make larger branched polymers and hence fewer chains. Very close to the gel point, theory expects the large branched polymers that control the terminal relaxation to relax by effective breakup, whereby the largest molecules break into two smaller molecules, and this type of break continues until the resulting pieces have Rouse motion faster than the effective breakup time. The relaxation time through effective breakup plus Rouse motion becomes faster than Rouse motion of the unbroken larger branched molecule. Rubinstein and Semenov say that creates a region very close to the gel point ($-\varepsilon_c < \varepsilon < \varepsilon_c$) where both the terminal modulus and relaxation time are constant (see Fig. 5b and c).[43,44]

Beyond the gel point (strictly speaking for $\varepsilon > \varepsilon_c$) the terminal modulus becomes the modulus of the unbroken network and is perfectly symmetric about the gel point (see Fig. 5b) up to $\varepsilon = 1$, where almost all chains attach to the gel and $G = \nu kT$, where ν is the number density of precursor chains (*i.e.* # of network strands ≈ # of precursor chains). For $\varepsilon > 1$ this terminal modulus simply grows proportional to ε as the network strands become shorter on average than the precursor chains. Hence the terminal modulus has six regimes of ε, each scaling as $G \sim |\varepsilon|^t$ (see Fig. 5b) with exponent $t = 3$ for mean field gelation ($-1 < \varepsilon < \varepsilon_G$ and $\varepsilon_G < \varepsilon < 1$), $t = 2.7$ for critical percolation ($-\varepsilon_G < \varepsilon < -\varepsilon_c$ and $\varepsilon_c < \varepsilon < \varepsilon_G$), $t = 0$ for the effective breakup regime very close to the gel point ($-\varepsilon_c < \varepsilon < \varepsilon_c$) and $t = 1$ for the fully developed network with $\varepsilon > 1$.[1,15]

The terminal relaxation time τ is only an increasing function of ε (more associations can only delay relaxation) with $\tau \sim |\varepsilon|^q$ with six regimes for the exponent q (see Fig. 5c). Below the gel point there are mean field percolation and critical percolation regimes that are identical to covalent crosslinking of unentangled precursor chains, with $q = -3$ for mean field percolation ($-1 < \varepsilon < -\varepsilon_G$) and $q = -4.0$ for critical percolation ($-\varepsilon_G < \varepsilon < -\varepsilon_c$). At $\varepsilon = -\varepsilon_c$ the relaxation time starts to be controlled by effective breakup and for all $\varepsilon > -\varepsilon_c$ breaking of associations controls the terminal relaxation time. In the effective breakup regime, Rubinstein and Semenov[43,44] expect the terminal time to be independent of ε, so $q = 0$ for $-\varepsilon_c < \varepsilon < \varepsilon_c$. For $\varepsilon > \varepsilon_c$ the longest relaxation time is controlled by the association lifetime and there are three regimes, with $q = 1.35$ for critical percolation ($\varepsilon_c < \varepsilon < \varepsilon_G$), $q = 1$ for mean field gelation ($\varepsilon_G < \varepsilon < 1$) and $q = 2$ for the fully developed gel with $\varepsilon > 1$.[15]

It is important to point out that none of the predicted values of exponents t and q have actually been confirmed in either experiment or simulation for associative polymers! In part, the reason is that there is always some error in the spectroscopy measures of the fraction of associative groups p that translates into the error in ε diverging as the gel point is approached. So that is an important future test for these models. In particular, the effective breakup idea very close to the gel point has not been tested at all. In what follows we present rheology data for two systems of associative polymers that each has one sample designed to be as close as possible to the gel point, but to test

this effective breakup idea, a minimum of two samples in the $-\varepsilon_c < \varepsilon < \varepsilon_c$ effective breakup regime very close to the gel point would be needed, making this idea best tested by simulation, where p and hence ε can be very carefully controlled.

In practice, instead of measuring exponents t and q, rheologists measure the linear viscoelastic response of associative polymers at various fixed p and hence ε. For samples that are as close as possible to the gel point ($\varepsilon = 0$ or $p = p_c$) that linear viscoelastic (LVE) response is very rich, as the theory expects to see four power laws in frequency for the storage modulus[15] G' (see Fig. 6) with $G' \sim \omega^u$. At very high frequency $\omega > 1/\tau_X$ where τ_X is the Rouse time of the precursor chains, LVE probes the motions on scales smaller than the linear precursor chains with $u = 1/2$ for their Rouse motions. For $\omega < 1/\tau_X$ the incipient gel has structures that correspond to mean field percolation on smaller scales, with $u = t/q = 1$, since $t = q = 3$ and on larger scales has structures corresponding to critical percolation with $u = t/q = 2.7/4.0 = 0.67$. Finally at the lowest frequencies below the reciprocal of the longest relaxation time, the exponent $u = 2$, corresponding to the terminal response of any viscoelastic liquid, as shown in blue in Fig. 6.

The precursor chains with no associative groups ($\varepsilon = -1$ or $p = 0$) just exhibit the linear chain Rouse part with $u = 1/2$ and then show terminal relaxation with $u = 2$ (black in Fig. 6). At the Ginzburg point below the gel point ($\varepsilon = -\varepsilon_G$) the LVE exhibits two power laws with $u = 1/2$ and 1 before the terminal response with $u = 2$ (orange). Below the gel point, as more associative groups are added (larger p and ε) the terminal relaxation time increases (Fig. 5c) and the terminal $G' \sim \omega^2$ progressively moves to a lower frequency. Beyond the gel point there is an associative network that exhibits a frequency independent modulus (the terminal modulus of Fig. 5b) that progressively increases with p and ε. That plateau starts at a progressively larger frequency and ends at a progressively lower frequency as p and ε increase. At higher frequencies than the plateau, the LVE is the same as the incipient gel and then shows a plateau in G' until the frequency that is the reciprocal of the longest relaxation time from Fig. 5c. Three examples are shown schematically in Fig. 6, at $\varepsilon = \varepsilon_G$ (green), at $\varepsilon = 1$ (red) and at $\varepsilon = 2$ (purple). For $0 < \varepsilon < 1$, the tenuous network goes to the terminal response with $u = 2$ directly from the plateau, while for $\varepsilon > 1$ there is a sticky Rouse relaxation mechanism with $u = 1/2$ between the plateau and the terminal response (the sticky Rouse model will be explained in the next section).

Although the associative polymers have been investigated since more than half a century ago, the strict examination of a sol-to-gel transition at a low content of stickers had not been given until very recently by Chen *et al.*[14,15,19,45,52–54] The precise synthesis of samples having a number of effective stickers per chain from 0 to 2 has been achieved for two model systems: the sulfonated polystyrene with different alkali counterions (SPS–X, with X = Na, K, Rb, or Cs), and the *n*-butyl acrylate (PnBA) based copolymers containing hydrogen bonding 2-ureido-4[1*H*]-pyrimidinone (UPy) groups as stickers (with chemical structures shown in the insets of Fig. 7).[14,16,55–57] Fig. 7 summarizes the evolution of LVE with an increase of the sticker content for (a) SPS–Na and (b) PnBA–UPy, where the symbols are the experimental results and curves are the prediction of the reversible gelation theory. In prediction of the LVE of SPS–Na, Chen *et al.* utilized all ionic groups as effective stickers.[15,52–54] In contrast, they utilized a prefactor of $f = 0.5$–0.7 to correct the number fraction of "effective" stickers of the PnBA–UPy system, meaning that not all the stickers form interchain associations. The prediction of the reversible gelation model agrees reasonably with the experimental results for both systems.[15,53,54] For the SPS–Na system, the 0.76 sample is very close to the gel point ($p_c = 1/(N-1) = 0.78$), enabling us to observe a clear Ginzburg transition from mean-field scaling $G' \sim \omega^1$ to critical percolation scaling $G' \sim \omega^{2/3}$. In contrast, the gel transition is expected to be between the 2.4 wt% and 3.4 wt% samples for the PnBA–UPy system, but no sample is sufficiently close to the gel point to enable a clear observation of the Ginzburg transition.

3.2 Sticky Rouse

Above the gel point but below the full gelation point (*i.e.* $0 < \varepsilon < 1$), the average size of a gel strand is larger than that of the precursor chain, meaning that the gel strand has a superbridged structure.

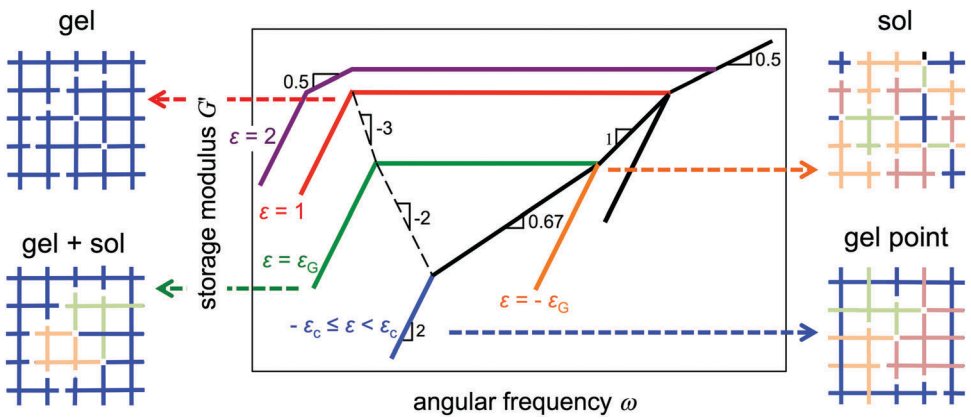

Fig. 6 Schematic of predicted evolution of storage modulus G' against frequency ω along with a sol–gel transition predicted by the reversible gelation model for unentangled associative polymers.[15] (logarithmic scales) The unconnected chains are represented in different colors.

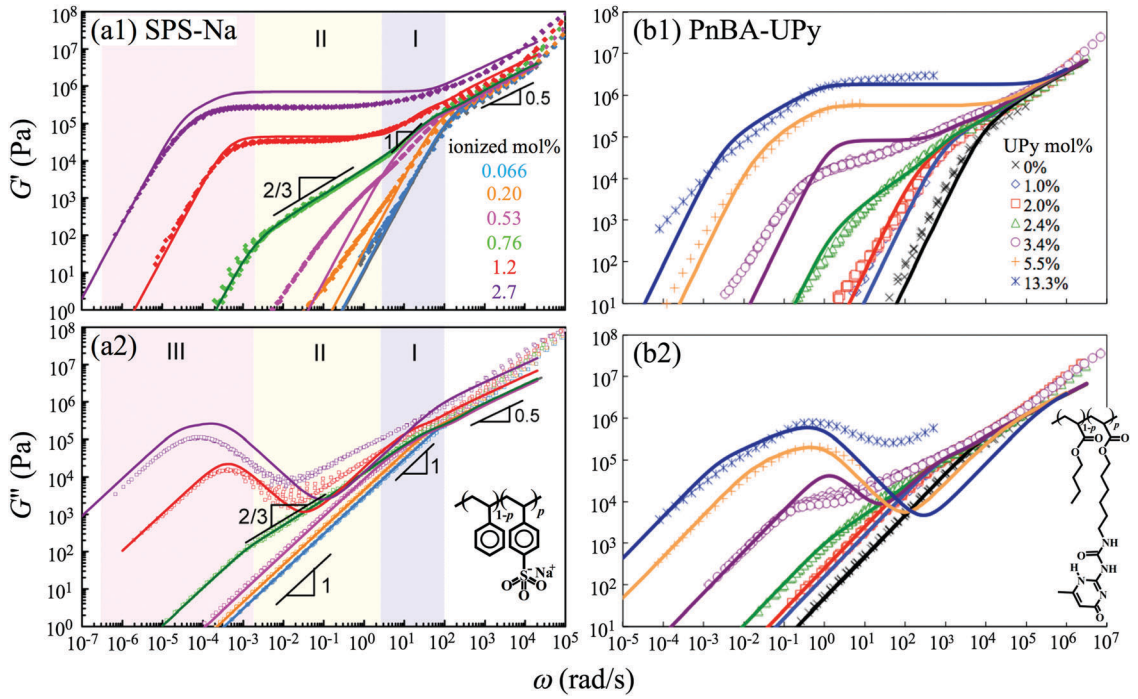

Fig. 7 Evolution of storage and loss moduli, G' and G'', against frequency ω along with a sol–gel transition in (a) an unentangled sulfonated polystyrene ionomer with a fraction of ionized monomer as indicated,[14,38] and (b) unentangled hydrogen bonding PnBA–UPy copolymers with a fraction of monomer containing the UPy groups as indicated. The symbols are the experimental results and the curves are predictions of the reversible gelation model.[16] The insets show the chemical structure of the samples.

For this case, the full relaxation of gel strands through effective breakup leads to the relaxation of the system as a whole.[43,44] In contrast, for $\varepsilon > 1$, the average size of the gel strands becomes smaller than that of the precursor chain. In other words, a precursor chain would weave within the gel network, and be divided into more than one network strand. For this case, relaxation of a strand would not lead to the relaxation of the system as a whole, because the orientational correlation still remains for the strands belonging to the same chain. The chain would relax through repeated breakup-association processes of all the stickers belonging to the same chain through the sticky-Rouse mechanism.[30,58–61] Before the breakup, a plateau can be observed on time scales shorter than the sticker lifetime τ_s if that lifetime is sufficiently long,

$$G = \frac{\rho RT}{M_s} \tag{6}$$

where M_s is an average molecular weight of the network strands. If the breakups of different stickers are independent events, the relaxation time of the chain would be Rouse-like $\tau \sim \tau_s(M/M_s)^2 \approx \tau_s\varepsilon^2$, the latter scaling is derived from $M/M_s \approx \varepsilon$ that holds for $\varepsilon > 1$.[30,43,59–61]

A test of the sticky Rouse model has been given on poly(ethylene oxide) based ionomers.[30,61] One benefit of this system is that the ionic groups are uniformly distributed and their dissociation can be simultaneously detected in the linear viscoelastic and dielectric measurements. Fig. 8 compares (a) storage and loss moduli, G' and G'', and (b) derivative formalism of the dielectric spectra, $\varepsilon_{der} = -\pi/2 \times \partial\varepsilon'(\omega)/\partial \ln \omega$, as functions of angular frequency ω for two PEO-ionomers at 20 °C. ε_{der} is usually used when ionic conductivity masks the low ω dielectric loss ε''.[62,63] In LVE (Fig. 8(a)), we defined the ionic dissociation frequency as a frequency ω_c where G' equals to $G_c = \rho RT/M_s$ (*cf.* eqn (6)). In dielectric relaxation spectroscopy (DRS) (Fig. 8(b)), an α process (thin solid curve), an α_2 process (thick solid curve), and an electrode polarization (dashed line) can be detected. The peak of the α process in DRS is close to the peak in G'' associated with the glass transition in LVE. Meanwhile, the peak frequency ω_{max} of the α_2 process agrees remarkably well with ω_c in LVE.[30] The agreement enables us to input the characteristic time of the α_2 relaxation (as τ_s) along with the molecular weight distribution into the sticky Rouse model to predict LVE of the ionomers remarkably well, as shown in the curves in Fig. 8(a).

The ionic groups of PEO-based ionomers can strongly coordinate with ethylene oxide, which makes the glass transition T_g increase greatly with the ion content. (In Fig. 8, a reduction of PEO spacer from M = 1100 to 600 results in an increase of the ion content.) Also due to this coordination, the ions do not aggregate as strongly, leading to no clear ionic peak (see Fig. 4(b)). The significant increase of T_g and weak association lead to subtle sticky Rouse LVE very similar to simple Rouse LVE and no visible plateau at the modulus of eqn (6). Recently, some research works showed that the agreement between ω_c and ω_{max} cannot be achieved in other systems, which suggested a possible difference between LVE detected ionic dissociation and dielectric detected ionic fluctuation,[16,64,65] attributed to stickers returning to the same association many times before finding a new association to join.[66] As will be detailed in Section IV, the unentangled PEO-Na

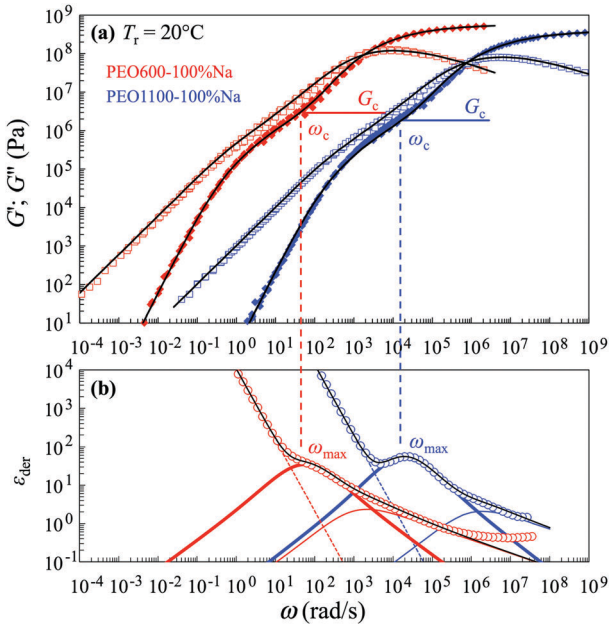

Fig. 8 (a) Master curves of storage and loss moduli, G' and G'', and (b) derivative formalism of dielectric spectra, ε_{der}, as functions of angular frequency ω for unentangled PEO600–100%Na (meaning there are M = 600 PEO chains between sulfonated phthalates; red) and PEO1100–100%Na (meaning there are M = 1100 PEO chains between sulfonated phthalates; blue) samples, at 20 °C. The characteristic modulus G_c evaluated from eqn (6) enables evaluation of the characteristic frequency ω_c from LVE. There are three processes detectable in DRS, the α process (thin solid curves), α_2 process (thick solid curves), and electrode polarization (dotted lines). The peak frequency of the α_2 process, ω_{max}, is close to ω_c in LVE, and the peak frequency of the α relaxation is close to the frequency where G'' has a peak in LVE associated with the glass transition.

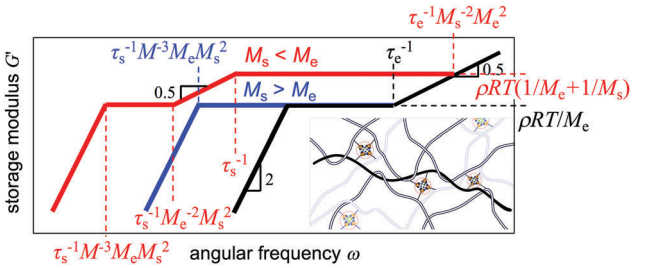

Fig. 9 Evolution of storage modulus G' against frequency ω along with a transition from the precursor (black lines) to $M_s > M_e$ (blue lines), and finally to $M_s < M_e$ (red lines), as predicted by the sticky reptation model (logarithmic scales).

ionomers in Fig. 8 have weak associations with energy ~10 kJ mol^{-1} and have no plateau at the modulus level of eqn (6). In contrast, unentangled PTMO-Na ionomers have association energy ~58 kJ mol^{-1} and exhibit a plateau at the modulus level of eqn (6) that spans nine decades in frequency.[30]

3.3 Sticky reptation

Similarly, for an entangled chain containing multiple interchain stickers, the chain relaxation can only be realized through reptation[67,68] triggered by repeated breakup-association processes of all the stickers belonging to it, *i.e.* the sticky-reptation mechanism. For this case, the amplitude of the plateau modulus before τ_s can be expressed as:[17]

$$G = \rho RT\left(\frac{1}{M_s}+\frac{1}{M_e}\right) \quad (7)$$

for long-chain ionomers, while for shorter chains there is the Flory end-correction,

$$G = \rho RT\left(\frac{1}{M_s}+\frac{1}{M_e}\right)\left(1-\frac{2M_s}{M}\right) \quad (8)$$

where the modulus amplitude is determined from both the network of the interchain associations, and that of entanglement. The chain relaxation mechanism should contain several subcases depending on the degree of association, and relative time scale of ion dissociation, entanglement relaxation, and chain reptation. Here, we explain only the two subcases that have been experimentally tested so far. The first subcase is $M_s > M_e$ (many entanglements on each associating network strand) and τ_s is much longer than the Rouse time of a strand of M_s. For this case, an effective sticker dissociation would allow a fraction M_s/M of the chain to reptate over a distance of $a(M_s/M_e)^{1/2}$ (where the lifetime of sticker is assumed to be much longer than the Rouse time of the strand), with a being the entanglement length. Then, the reptation time of the whole chain over a contour length of $L = aM/M_e$ becomes $\tau_{rep} = \tau_s M^3 M_e^{-1} M_s^{-2}$. The second subcase is $M_s < M_e$ (many associations on each entanglement strand) and τ_s is much longer than the Rouse time of a strand of molecular weight M_s. For this case, the equilibration of an entanglement strand is through the sticky Rouse mechanism to give $\tau_e = \tau_s M_e^2/M_s^2$, and accordingly the sticky reptation time is $\tau_{rep} = \tau_e(M/M_e)^3 = \tau_s M^3 M_e^{-1} M_s^{-2}$, identical to that of the first subcase.[17,69] The scaling properties of these two subcases are summarized in Fig. 9, where the inset schematically shows an entangled associative polymer system containing both entanglement and associative networks. Although the expression of the reptation time is the same for the two subcases, the relaxation behavior is completely different: the drop in modulus at $1/\tau_s$ becomes negligible for the case with more entanglements than stickers ($M_s > M_e$, blue lines), while the classical Leibler double plateau[17] holds if there are more stickers than entanglements ($M_s < M_e$, red lines) with the higher frequency plateau given by eqn (7) and the lower frequency plateau $G = \rho RT/M_e$ from entanglements alone.

Fig. 10 compares LVE of PS based ionomers corresponding to (a) subcase 1 ($M_s > M_e$) and (b) subcase 2 ($M_s < M_e$), respectively. In panel (a) where $M_s > M_e$, the equilibration of an entanglement segment is not strongly affected by the sticker dissociation, and thus the plateau amplitude is similar to that of the precursor chain, while the sticky-reptation time is more delayed for chains containing more stickers. In panel (b) where $M_s < M_e$, the equilibration over the entanglement length is through a sticky-Rouse mechanism, leading to the formation of the high ω plateau with modulus given by eqn (7).[70] Since all the samples have a similar ion content (~4%) in Fig. 10(b), the high ω plateaus have the same amplitude. The non-entangled

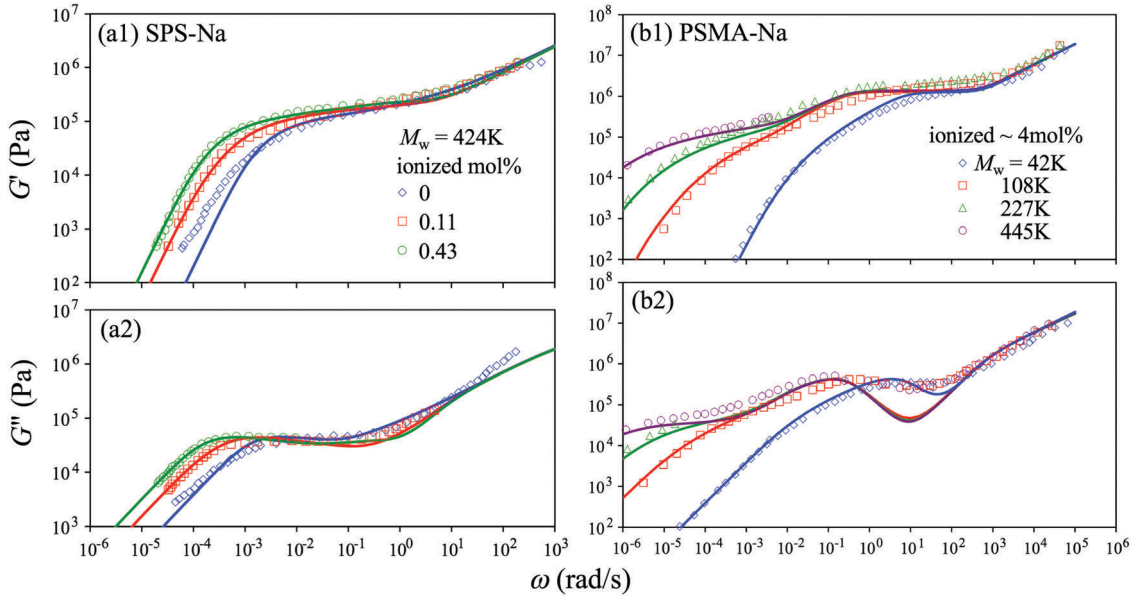

Fig. 10 (a) Entangled sulfonated polystyrene of having M_w = 424 000 g mol^{-1} and a number of ions much lower than that of entanglements,[70] and (b) non-entangled (M_w = 42 000 g mol^{-1}) and three entangled (M_w > 100 000 g mol^{-1}) copolymers of styrene and methacrylic acid with sodium counterions,[71] with number density of ions of the entangled samples higher than that of the entanglements. The curves are predictions from the sticky-double-reptation model.[18]

42 000 g mol^{-1} sample relaxes through a sticky-Rouse mechanism (M_w/M_e = 2.5 is too small for entanglement effects). In contrast, a second low-ω plateau shows up for the other three samples having M_w > 100 000 g mol^{-1} that are well entangled, and the terminal relaxation through the sticky reptation mechanism is more delayed for samples having larger M.[71]

The curves in Fig. 10 are predictions based on a sticky double reptation model that considers an entanglement as a two-chain event, and its relaxation can be realized when a chain end of one of the two chains diffuses away.[18,72–80] The necessity of introducing the double reptation is because both the chain length and number of stickers per chain exhibit certain distributions, which greatly widens the distribution of relaxation rates of the associative chains. An alternative choice to treat the multiple-chain interaction through introducing a constraint release mechanism (or tube dilation mechanism) in a self-consistent manner.[78,79,81]

IV. Strength of association of associative polymers

The activation energy E_a of sticker dissociation is the most important parameter for associative polymers. The energy is usually written as:[16,19,30,43]

$$\tau_s = \tau_0 \exp(E_a/kT) \quad (9)$$

τ_0 is an attempt time for thermal motion, taken as the segment motion time scale without stickers, but reflects any change in T_g that the stickers imparted to the segments. Eqn (9) means that the ionic dissociation time τ_s depends on a competition between an enthalpic attraction, of energy E_a, that keeps the sticker in the association, and the thermal motion, of energy kT, that tends to dissociate it. Although the expression of eqn (9) is quite straightforward, the experimental determination of the associating energy is challenging, due to the complicated relationship between the ionic dissociation time τ_s, and the terminal relaxation time τ that is detected directly in rheology, as discussed in the previous section.

To explain the relationship, we redraw Fig. 6 in a different way in Fig. 11, where the green and blue lines correspond to

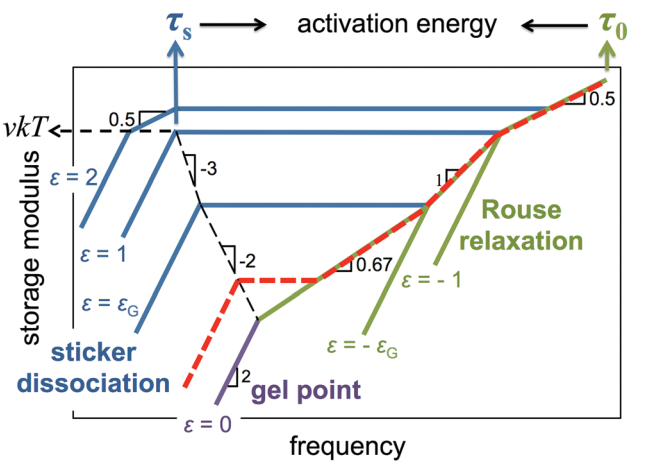

Fig. 11 Stress relaxation originating from Rouse motion (green lines) and sticker dissociation (blue lines) for unentangled associative polymers, where τ_0 corresponds to $G' \sim \nu_{Kuhn}kT$ of the Rouse region, and τ_s corresponds to the relaxation time at the full gelation point (ε = 1) where plateau modulus $G' \sim \nu kT$ (logarithmic scales).

stress relaxation originating from thermal motion and sticker dissociation, respectively. The latter occurs as a plateau for the samples above the gel point. In Fig. 11, τ_0 corresponds to a frequency of $G' \sim \nu_{Kuhn}kT$ in the Rouse regime where $G' \sim \omega^{0.5}$, with ν_{Kuhn} being the number density of Kuhn segments,[82,83] and τ_s corresponds to the terminal relaxation time at the full gelation point (because a chain contains two effective stickers on average, and thus the dissociation time of one of the stickers would immediately lead to the chain relaxation, assuming that the Rouse time is much shorter than the sticker lifetime), where the plateau modulus $G' \sim \nu kT$, with ν being the number density of precursor chains. This analysis is based on unentangled systems, for which the relationship between the terminal relaxation time and τ_s is more straightforward than the entangled systems.

With a ratio of τ_0 and τ_s obtained at any given T, E_a can be determined directly from eqn (9). Chen *et al.* noted that E_a determined from a ratio of τ_s/τ_0 at given T (with τ_s and τ_0 determined from fitting LVE to the reversible gelation model, as shown in Fig. 7) is much smaller than that determined directly from the temperature dependence of viscosity, or LVE shift factors. To address this disagreement, Chen *et al.* proposed that it is the temperature dependence of the ratio τ_s/τ_0, rather than that of either τ_s or τ_0 that is directly related to E_a.[16,19]

To test this idea requires a simultaneous measurement of the temperature dependence of both τ_s and τ_0 over a wide temperature range. To fulfill this requirement, a model sample can be chosen as a sample slightly above the gel point, see red lines in Fig. 11. The sample should exhibit stress relaxation originating from both the Rouse motion and the sticker dissociation that are not widely separated in time (but should be sufficiently separated to ensure that each of them exhibits its own T dependence), so that both can be measured within isothermal frequency sweeps over a certain T range.[16,19]

Fig. 12 shows the modulus obtained over a wide T range for the model PnBA–UPy hydrogen bonding samples. The modulus can be either shifted through superposing high-ω G'' stemming

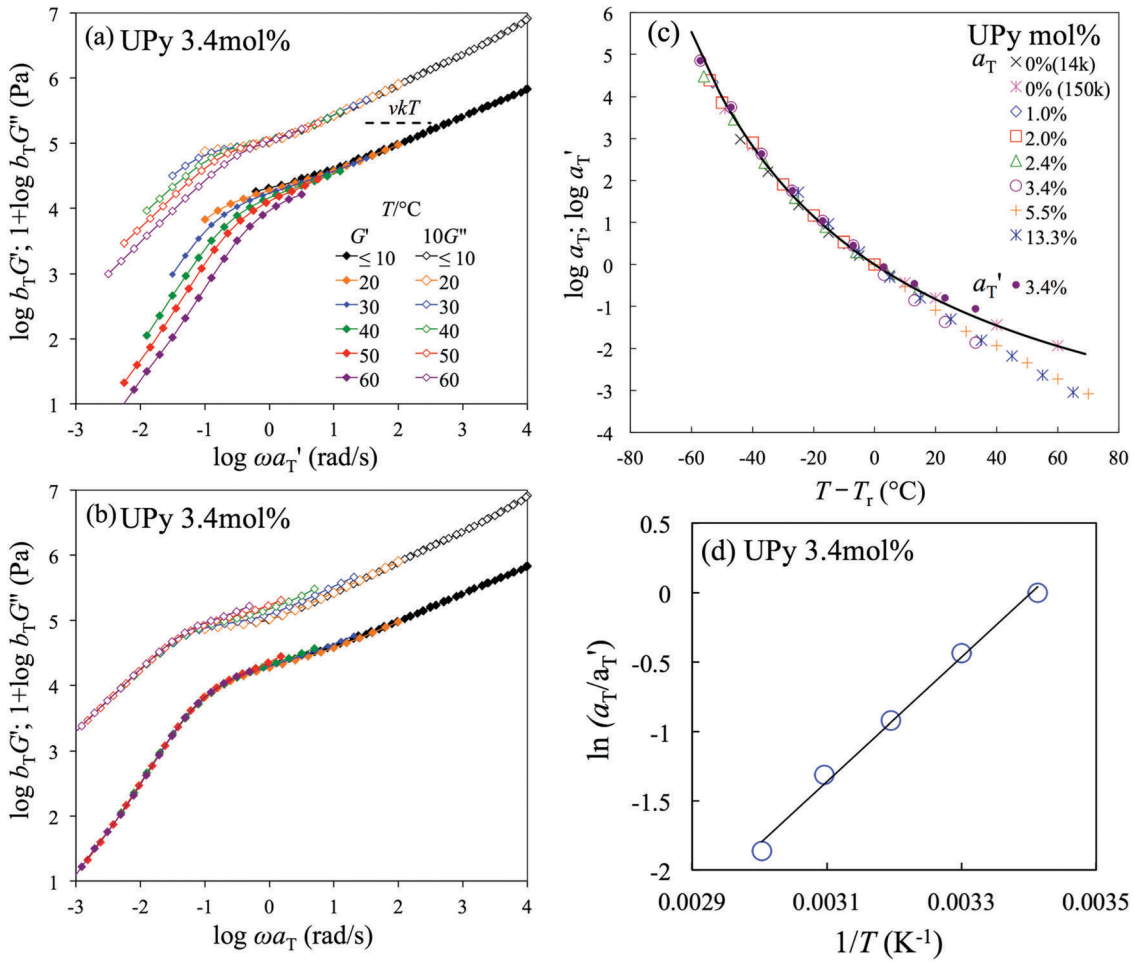

Fig. 12 For a PnBA–UPy sample with a fraction of UPy containing monomers of 3.4 mol%, the G' and G'' data are corrected by a temperature factor $b_T = T_r/T$, and shifted under the guidance of (a) a high-ω Rouse region of G'' and (b) a low-ω terminal sticker dissociation region of G'. (c) Comparison of the shift factors obtained in panels (a) and (b), *i.e.* a_T' and a_T, and shift factors for samples having higher or lower UPy contents. (d) Plot of the natural logarithm of the ratio of shift factors a_T/a_T' against $1/T$, enables calculation of activation energy E_a, since a_T/a_T' reflects the temperature dependence of τ_s/τ_0, making the slope E_a/k (see eqn (9)).

from the Rouse motion (panel a) or low-ω G' data stemming from the sticker dissociation (panel b), to determine the temperature dependencies of τ_0 and τ_s, respectively.[16,19] Panel (c) compares shift factors, a_T' and a_T, obtained from the two shifting methods of the model sample having 3.4 mol% UPy and those for samples below (with UPy mol% $<$ 3.4%) and well above (with UPy mol% $>$ 3.4%) the gel point. It is clear that a_T' of the 3.4 mol%UPy sample agrees well with those of samples below the gel point, for which the relaxation is governed by the Rouse motion. In contrast, a_T of the 3.4 mol%UPy sample agrees with those of the samples well above the gel point, for which the ionic dissociation governs the stress relaxation. Fig. 12(d) determines E_a through linear fitting of plots of the natural logarithm of the ratio of shift factors a_T/a_T' against $1/T$. Similar plots were also constructed for sulfonated PS ionomers with different counterions slightly above their gel points.[16,19]

The reference temperature T_r = 20 °C in Fig. 12(a) and (b) is chosen because both the high and low frequency moduli, corresponding respectively to the Rouse motion and ionic dissociation, can be commonly detected there. Based on this criterion, 30, 40, and 50 °C can also be chosen as T_r. Then, a natural question is: can E_a be consistently determined if a different T_r is chosen? At first glance, the method based on τ_s/τ_0 at T_r could be problematic, because $E_a = kT_r \ln(\tau_s/\tau_0)$ changes with T_r if τ_s/τ_0 remains the same. Nevertheless, it should be stressed that τ_s/τ_0 also changes with T_r, which distinguishes associative polymers from polymers without associating groups. To explain this point, let us take a look at Fig. 12(a), in which the high frequency data are superposed and accordingly τ_0 has been properly normalized. After the normalization, the terminal relaxation time governed by τ_s accelerates with increasing T. In other words, the relaxation mode distribution narrows with increasing T due to a reduction of E_a/T_r with increasing T_r. Therefore, $E_a = kT_r \ln(\tau_s/\tau_0)$ can be consistently determined here even if T_r is increased, because this increase would be cancelled out by a decrease of τ_s/τ_0 as T_r is increased. This idea has been explained in more detail in ref. 19.

Fig. 13 compares E_a determined from these two methods, which agree remarkably well for both the hydrogen bonding PnBA–UPy and the sulfonated polystyrene SPS–X systems, meaning that the energy can be consistently determined from both the absolute values of τ_0 and τ_s and from the temperature dependence of their ratio. The increase of E_a with decreasing counterion size for sulfonated PS ionomers (from Cs to Na) can be rationalized by considering the Coulomb energy $E = e^2/(\varepsilon\varepsilon_0 r)$: a reduction of the counterion size reduces the distance r between charges in the contact ion pair and thus increases the activation energy. The hydrogen bonding system PnBA–UPy has significantly smaller E_a than the ionomers, as expected. For comparison, the activation energy E_a evaluated from $\tau_{\alpha 2}/\tau_\alpha$ for PEO-Na and from τ_c/τ_α for PTMO-Na are added to Fig. 13 as arrows,[30] where $\tau_{\alpha 2} = 1/\omega_{max}$ for the α_2 relaxation, $\tau_\alpha = 1/\omega_{max}$ for the α relaxation, and $\tau_c = 1/\omega_c$, with ω_{max} and ω_c being explained earlier in Fig. 8. (We do not use $\tau_{\alpha 2}/\tau_\alpha$ for PTMO-Na because the α_2 and α processes are so well separated that they cannot both be measured at any single T.) Both $\tau_{\alpha 2}/\tau_\alpha$ and τ_c/τ_α can be regarded as reasonable approximations of τ_s/τ_0. Obviously, the weakly associating PEO-Na ionomers exhibit an association energy much smaller than the other samples that can be regarded as strong associative polymers.

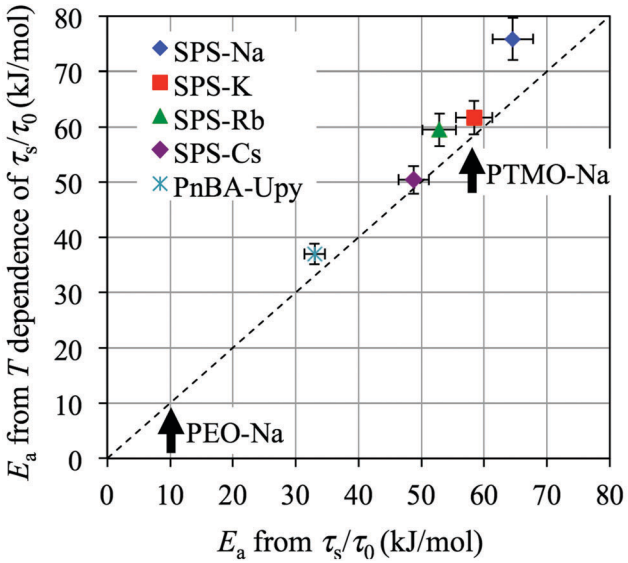

Fig. 13 Comparison of E_a determined directly from the ratio τ_s/τ_0 at any given T, and those from the temperature dependence of τ_s/τ_0 in a wide T range. The activation energy evaluated from $\tau_{\alpha 2}/\tau_\alpha$ for PEO-Na at T = 20 and τ_c/τ_α for PTMO-Na at T = are added as arrows for comparison.

V. Conclusion and future directions

The dynamics of associative polymers has been a subject of intensive research recently, due to its importance in developing varied functional materials with broad applications.[4] This review focused on recent progress in understanding the dynamics of associative polymers with randomly placed stickers. The density and strength of the associative groups, as well as the length of the polymer chains, play big roles in the dynamics of associating polymers. The formation of an associative network occurs at a very low ion content, ~one interchain sticker per chain. Near this gel point, the associative polymers exhibit very rich rheology (see Fig. 6). Although molecular theories can describe well the linear viscoelastic behavior of associative polymers, by considering both density and strength of sticker associations, the dynamics of associative polymers is still far from being fully understood.

First, the molecular details of the sticker dissociation are not well understood thus far. One of the biggest challenges is the lack of knowledge of the structure of clusters/aggregates of the stickers in real space. Taking ionomers as an example, the ion aggregation usually contains 5–10 ionic groups separated at a correlation spacing of 3–5 nm, which is close to the resolution limit of any state-of-the-art electron microscopy tools.[8,84,85] In sulfonated hydrocarbon ionomers, the ionized monomers (with high aggregation energy) can be treated as monomers highly repulsive from neutral monomers and attractive to themselves,[86,87]

which is an over-simplified molecular picture that neglects the localized electrostatic interaction of the ionic aggregate.[88] In sulfonated PEO ionomers, the ether oxygen has roughly half of the interaction energy with small cations than the sulfonate has, creating more open "ion chain" aggregates.[89] To understand the aggregate structure would be the first step to reveal the molecular details related to the sticker dissociation. The traditional molecular view for the sticker dissociation is "hopping" of stickers from one cluster/aggregate to another.[8,90–92] Rubinstein pointed out that the hopping is not a one-step event, the sticker may need to return back to the original cluster/aggregate many times before it finds a new partner.[66] Wang recently pointed out that such a hopping of ions could face an energy barrier higher than that for two clusters/aggregates to encounter and exchange stickers.[93]

To check the molecular details of the dissociation, one possible experimental model system is associative polymers with a precisely controlled sticker position, *e.g.* the "periodic" associative polymers[94–98] having identical polymer spacers between stickers, which could be synthesized through cyclic diene metathesis (ADMET) polymerization.[99,100] The precise placement of stickers could result in a well-controlled aggregation morphology, *e.g.* the cubic lattice arrangement of ionic aggregates,[98] and accordingly facilitate the discussion of ionic spacing. (The PEO and PTMO ionomers in Fig. 4 are close to this precise limit but not strictly "periodic" considering that the PEO and PTMO spacers exhibit a certain distribution of M with $M_w/M_n \sim 1.1$.[31,101])

Second, associative polymers often have more than one type of interaction that enables dissipation of energy on varied time scales.[52,53] For hydrocarbon ionomers, there is only one primary Coulomb interaction and ion aggregates are expected to be dense, meaning that the stickers in the interior of the aggregate may have a longer association lifetime than the stickers on the aggregate surface. For ethylene oxide ionomers there is a strong interaction between ether oxygen and small cations that complicates their dynamics. For the UPy polymers, there are other hydrogen bond receptors on the acrylate groups. For ionomers, the association energy can be controlled by the counterion type and thus one simple approach is to mix different types of ions to tune the energy dissipation distribution. For example, ionomers used for golf ball covers usually contain more than one type of counterion (Na, K, Zn and so on), which allows the golf ball to exhibit high toughness and impact resistance under varied weather conditions.[4] Recently, the double network gels have attracted a great amount of attention, the basic concept of one sacrificial network and the other network to sustain the structure[102] should be applicable also to associative polymers with two distinct types of associations.

Third, the studies summarized in this review cover only limited cases with respect to the density of stickers and entanglements. For example, all the discussions of entangled associative polymers in this review are based on the sticky-reptation model, which should hold when each entangled chain has two stickers or more. In an opposite case where the ion content is very low, there should also be a sol-to-gel transition, in principle. Above the gel point, if there are considerable numbers of chains that have only one sticker or no sticker, these chains would relax through arm retraction and reptation, respectively, as pointed out by van Ruymbeke and coworkers.[81] The relaxed chains may serve as a diluent for the network formed by chains having two or more stickers. Even when the chains are all associated, the entanglement relaxation is still not uniform if the number of stickers is much smaller than that of the entanglements: a fraction of entanglements near the chain ends could relax first, through arm retraction, constraint release and so on, and the remaining entanglements trapped by the long lifetime stickers would relax later. For this case, a double plateau behavior is expected: the high frequency plateau has amplitude comparable to the entanglement plateau, and the low frequency plateau is lower, whose amplitude depends on the number of trapped entanglements[1] in the associative network. To fully test the entanglement relaxation for these transitional cases are considered as an interesting future subject.

Finally, to understand the nonlinear rheology is even more challenging in both the experimental and theoretical aspects. Several nonlinear phenomena, including shear-thickening,[103,104] strain hardening,[105–107] wall slip,[107] shear-banding, and fracture,[108] which have been reported for associative polymers under strong shear/elongational flows are far from being well-understood, and even under intense debate.[107,109] Take the shear-thickening phenomenon as an example; it usually shows up before shear thinning in associative polymers with a loose network, like a superbridged network of telechelic chains or ionomers near the gel point.[54,103,104] This phenomenon has been attributed to mechanisms including finite extensible nonlinear elasticity (FENE), and the flow-induced increase of intermolecular associations.[103,104,110–112] Nevertheless, no single mechanism seems to be able to explain all the experimental phenomena.[54,113] Newly developed experimental tools and techniques should improve the measurements and thus contribute to a better understanding of the nonlinear rheology of associative polymers, which include the cone-partitioned plate that reduces the edge fracture effect,[114] the fibril extensional rheometer that measures real extensional strain and stress,[115] thanks to the *in situ* tracking of the fibril shape, the surface-modified technique that can reduce slip,[116] and a particle tracking technique that can quantify any change of flow uniformity.[117] Such methods show great promise for future studies of the nonlinear rheology of both associative and non-associating polymers.

Conflicts of interest

There are no conflicts to declare.

Acknowledgements

QC acknowledges the National Natural Science Foundation of China (21722407 and 21674117), and the "Thousand Youth Talents Plan" program. RHC acknowledges the National Science Foundation, Division of Materials Research Polymers Program (Grant DMR-1404586).

References

1 M. Rubinstein and R. H. Colby, *Polymer Physics*, Oxford University Press, New York, 2003.
2 J. N. Israelachvili, *Intermolecular and surface forces*, Academic Press, Burlington, MA, 3rd edn, 2011.
3 A. Y. Grosberg and A. R. Khokhlov, *Giant molecules here, there, and everywhere*, World Scientific, Hackensack, NJ, 2nd edn, 2011.
4 L. H. Zhang, N. R. Brostowitz, K. A. Cavicchi and R. A. Weiss, *Macromol. React. Eng.*, 2014, **8**, 81–99.
5 L. R. Middleton and K. I. Winey, *Annu. Rev. Chem. Biomol. Eng.*, 2017, **8**, 499–523.
6 M. B. Jackson, *Molecular and cellular biophysics*, Cambridge University Press, New York, 2006.
7 E. van Ruymbeke, *J. Rheol.*, 2017, **61**, 1099–1102.
8 A. Eisenberg and J.-S. Kim, *Introduction to Ionomers*, Wiley, New York, 1998.
9 A. Eisenberg and M. Rinaudo, *Polym. Bull.*, 1990, **24**, 671.
10 A. V. Dobrynin and M. Rubinstein, *Prog. Polym. Sci.*, 2005, **30**, 1049–1118.
11 P. G. de Gennes, P. Pincus, R. M. Velasco and F. Brochard, *J. Phys.*, 1976, **37**, 1461–1473.
12 P. Dubin, *Macromolecular Complexes in Chemistry and Biology*, Springer-Verlag, Berlin, New York, 1994.
13 Q. Chen, N. Bao, J.-H. H. Wang, T. Tunic, S. Liang and R. H. Colby, *Macromolecules*, 2015, **48**, 8240–8252.
14 Z. Zhang, C. Liu, X. Cao, J.-H. H. Wang, Q. Chen and R. H. Colby, *Macromolecules*, 2017, **50**, 963–970.
15 Q. Chen, C. W. Huang, R. A. Weiss and R. H. Colby, *Macromolecules*, 2015, **48**, 1221–1230.
16 Z. J. Zhang, C. Liu, X. Cao, L. C. Gao and Q. Chen, *Macromolecules*, 2016, **49**, 9192–9202.
17 L. Leibler, M. Rubinstein and R. H. Colby, *Macromolecules*, 1991, **24**, 4701–4707.
18 Q. Chen, Z. J. Zhang and R. H. Colby, *J. Rheol.*, 2016, **60**, 1031–1040.
19 Z. Zhang, C. Huang, R. A. Weiss and Q. Chen, *J. Rheol.*, 2017, **61**, 1199–1207.
20 R. D. Lundberg and R. R. Phillips, *J. Polym. Sci., Polym. Phys. Ed.*, 1982, **20**, 1143–1154.
21 C. W. Lantman, W. J. Macknight, J. S. Higgins, D. G. Peiffer, S. K. Sinha and R. D. Lundberg, *Macromolecules*, 1988, **21**, 1339–1343.
22 C. W. Lantman, W. J. Macknight, D. G. Peiffer, S. K. Sinha and R. D. Lundberg, *Macromolecules*, 1987, **20**, 1096–1101.
23 J. Wang, Z. L. Wang, D. G. Peiffer, W. J. Shuely and B. Chu, *Macromolecules*, 1991, **24**, 790–798.
24 K. Chakrabarty, P. Shao and R. A. Weiss, in *Ionomers: Synthesis, Structure, Properties and Applications*, ed. M. R. Tant, K. A. Mauritz and G. L. Wilkes, Blackie Academic & Professional, London, New York, 1st edn, 1997, pp. 158–207.
25 S. Jousset, H. Bellissent and J. C. Galin, *Macromolecules*, 1998, **31**, 4520–4530.
26 M. Hara, in *Physical Chemistry of Polyelectrolytes*, ed. T. Radeva, Marcel Dekker, New York, 2001, pp. 245–279.
27 A. Sehgal and T. A. P. Seery, *Macromolecules*, 2003, **36**, 10056–10062.
28 A. M. Castagna, W. Q. Wang, K. I. Winey and J. Runt, *Macromolecules*, 2011, **44**, 5420–5426.
29 W. Wang, G. J. Tudryn, R. H. Colby and K. I. Winey, *J. Am. Chem. Soc.*, 2011, **133**, 10826–10831.
30 Q. Chen, G. J. Tudryn and R. H. Colby, *J. Rheol.*, 2013, **57**, 1441–1462.
31 G. J. Tudryn, M. V. O'Reilly, S. C. Dou, D. R. King, K. I. Winey, J. Runt and R. H. Colby, *Macromolecules*, 2012, **45**, 3962–3973.
32 J.-H. H. Wang, C. H. Yang, H. Masser, H.-S. Shiau, M. V. O'Reilly, K. I. Winey, J. Runt, P. Painter and R. H. Colby, *Macromolecules*, 2015, **48**, 7273–7285.
33 S. Liang, M. V. O'Reilly, U. H. Choi, H.-S. Shiau, J. Bartels, Q. Chen, J. Runt, K. I. Winey and R. H. Colby, *Macromolecules*, 2014, **47**, 4428–4437.
34 M. V. O'Reilly, H. Masser, D. R. King, P. C. Painter, R. H. Colby, K. I. Winey and J. Runt, *Polymer*, 2015, **59**, 133–143.
35 Q. Chen, *Acta Polym. Sin.*, 2017, 1220–1233.
36 A. Eisenberg, B. Hird and R. B. Moore, *Macromolecules*, 1990, **23**, 4098–4107.
37 A. M. Castagna, W. Wang, K. I. Winey and J. Runt, *Macromolecules*, 2010, **43**, 10498–10504.
38 A. M. Castagna, W. Q. Wang, K. I. Winey and J. Runt, *Macromolecules*, 2011, **44**, 2791–2798.
39 M. B. Armand, *Annu. Rev. Mater. Sci.*, 1986, **16**, 245–261.
40 M. Armand and J. M. Tarascon, *Nature*, 2008, **451**, 652–657.
41 W. W. Huang, R. Frech and R. A. Wheeler, *J. Phys. Chem.*, 1994, **98**, 100–110.
42 O. Borodin and G. D. Smith, *Macromolecules*, 2006, **39**, 1620–1629.
43 M. Rubinstein and A. N. Semenov, *Macromolecules*, 1998, **31**, 1386–1397.
44 A. N. Semenov and M. Rubinstein, *Macromolecules*, 1998, **31**, 1373–1385.
45 Q. Chen and R. H. Colby, *Korea–Aust. Rheol. J.*, 2014, **26**, 257–261.
46 M. Rubinstein and R. H. Colby, *Macromolecules*, 1994, **27**, 3184–3190.
47 P. G. de Gennes, *J. Phys., Lett.*, 1977, **38**, L355–L358.
48 Y. Matsumiya, H. Watanabe, O. Urakawa and T. Inoue, *Macromolecules*, 2016, **49**, 7088–7095.
49 Y. Kwon, Y. Matsumiya and H. Watanabe, *Macromolecules*, 2016, **49**, 3593–3607.
50 H. Watanabe, Y. Matsumiya, Y. Masubuchi, O. Urakawa and T. Inoue, *Macromolecules*, 2015, **48**, 3014–3030.
51 M. E. Cates, *J. Phys., Lett.*, 1985, **46**, L837–L843.
52 C. W. Huang, Q. Chen and R. A. Weiss, *Macromolecules*, 2017, **50**, 424–431.
53 C. W. Huang, C. Wang, Q. Chen, R. H. Colby and R. A. Weiss, *Macromolecules*, 2016, **49**, 3936–3947.
54 C. W. Huang, Q. Chen and R. A. Weiss, *Macromolecules*, 2016, **49**, 9203–9214.

55 K. E. Feldman, M. J. Kade, E. W. Meijer, C. J. Hawker and E. J. Kramer, *Macromolecules*, 2011, **44**, 5537.
56 K. E. Feldman, M. J. Kade, E. W. Meijer, C. J. Hawker and E. J. Kramer, *Macromolecules*, 2010, **43**, 3576.
57 K. E. Feldman, M. J. Kade, E. W. Meijer, C. J. Hawker and E. J. Kramer, *Macromolecules*, 2009, **42**, 9072–9081.
58 M. S. Green and A. V. Tobolsky, *J. Chem. Phys.*, 1946, **14**, 80–92.
59 L. G. Baxandall, *Macromolecules*, 1989, **22**, 1982–1988.
60 Q. Chen, H. Masser, H.-S. Shiau, S. Liang, J. Runt, P. C. Painter and R. H. Colby, *Macromolecules*, 2014, **47**, 3635–3644.
61 Q. Chen, S. Liang, H.-S. Shiau and R. H. Colby, *ACS Macro Lett.*, 2013, **2**, 970–974.
62 J. van Turnhout and M. Wubbenhorst, *J. Non-Cryst. Solids*, 2002, **305**, 50–58.
63 M. Wubbenhorst and J. van Turnhout, *J. Non-Cryst. Solids*, 2002, **305**, 40–49.
64 B. J. Gold, C. H. Hövelmann, N. Lühmann, N. K. Székely, W. Pyckhout-Hintzen, A. Wischnewski and D. Richter, *ACS Macro Lett.*, 2017, **6**, 73–77.
65 A. Shabbir, I. Javakhishvili, S. Cerveny, S. Hvilsted, A. L. Skov, O. Hassager and N. J. Alvarez, *Macromolecules*, 2016, **49**, 3899–3910.
66 E. B. Stukalin, L. H. Cai, N. A. Kumar, L. Leibler and M. Rubinstein, *Macromolecules*, 2013, **46**, 7525–7541.
67 P. G. de Gennes, *J. Chem. Phys.*, 1971, **55**, 572–579.
68 M. Doi, *Introduction to polymer physics*, Oxford University Press, New York, 1996.
69 R. H. Colby, X. Zheng, M. H. Rafailovich, J. Sokolov, D. G. Peiffer, S. A. Schwarz, Y. Strzhemechny and D. Nguyen, *Phys. Rev. Lett.*, 1998, **81**, 3876–3879.
70 R. A. Weiss and W. C. Yu, *Macromolecules*, 2007, **40**, 3640–3643.
71 J. S. Kim, K. Yoshikawa and A. Eisenberg, *Macromolecules*, 1994, **27**, 6347–6357.
72 W. W. Graessley, *Adv. Polym. Sci.*, 1982, **47**, 67–117.
73 H. Watanabe, *Prog. Polym. Sci.*, 1999, **24**, 1253–1403.
74 H. Watanabe, Y. Matsumiya, Q. Chen and W. Yu, in *Polymer Science: A Comprehensive Reference*, ed. K. Matyjaszewski and M. Möller, Elsevier, Amsterdam, 2012, vol. 2, pp. 683–722.
75 T. C. B. McLeish, *Adv. Phys.*, 2002, **51**, 1379–1527.
76 J. Descloizeaux, *Macromolecules*, 1990, **23**, 4678–4687.
77 W. W. Graessley, *Polymeric Liquids and Networks: Dynamics and Rheology*, Garland Science, London, New York, 2008.
78 H. Goldansaz, C. A. Fustin, M. Wubbenhorst and E. van Ruymbeke, *Macromolecules*, 2016, **49**, 1890–1902.
79 M. Ahmadi, L. G. D. Hawke, H. Goldansaz and E. van Ruymbeke, *Macromolecules*, 2015, **48**, 7300–7310.
80 E. van Ruymbeke, R. Keunings, V. Stephenne, A. Hagenaars and C. Bailly, *Macromolecules*, 2002, **35**, 2689–2699.
81 L. G. D. Hawke, M. Ahmadi, H. Goldansaz and E. van Ruymbeke, *J. Rheol.*, 2016, **60**, 297–310.
82 T. Inoue, H. Okamoto and K. Osaki, *Macromolecules*, 1991, **24**, 5670–5675.
83 T. Inoue, Y. Mizukami, H. Okamoto, H. Matsui, H. Watanabe, T. Kanaya and K. Osaki, *Macromolecules*, 1996, **29**, 6240–6245.
84 K. M. Beers and N. P. Balsara, *ACS Macro Lett.*, 2012, **1**, 1155–1160.
85 B. P. Kirkmeyer, R. A. Weiss and K. I. Winey, *J. Polym. Sci., Polym. Phys.*, 2001, **39**, 477–483.
86 I. A. Nyrkova, A. R. Khokhlov and M. Doi, *Macromolecules*, 1993, **26**, 3601–3610.
87 A. N. Semenov, I. A. Nyrkova and A. R. Khokhlov, *Macromolecules*, 1995, **28**, 7491–7500.
88 L. R. Middleton and K. I. Winey, *Annu. Rev. Chem. Biomol. Eng.*, 2017, **8**, 499–523.
89 K. R. Lu, J. F. Rudzinski, W. G. Noid, S. T. Milner and J. K. Maranas, *Soft Matter*, 2014, **10**, 978–989.
90 P. Vanhoorne and R. A. Register, *Macromolecules*, 1996, **29**, 598–604.
91 X. Qiao and R. A. Weiss, *Macromolecules*, 2013, **46**, 2417–2424.
92 B. L. Papke, M. A. Ratner and D. F. Shriver, *J. Electrochem. Soc.*, 1982, **129**, 1694–1701.
93 D. Amin, A. E. Likhtman and Z. Wang, *Macromolecules*, 2016, **49**, 7510–7524.
94 C. F. Buitrago, K. L. Opper, K. B. Wagener and K. I. Winey, *ACS Macro Lett.*, 2012, **1**, 71–74.
95 L. R. Middleton, S. Szewczyk, J. Azoulay, D. Murtagh, G. Rojas, K. B. Wagener, J. Cordaro and K. I. Winey, *Macromolecules*, 2015, **48**, 3713–3724.
96 L. R. Middleton, E. B. Trigg, E. Schwartz, K. L. Opper, T. W. Baughman, K. B. Wagener and K. I. Winey, *Macromolecules*, 2016, **49**, 8209–8218.
97 E. B. Trigg, M. J. Stevens and K. I. Winey, *J. Am. Chem. Soc.*, 2017, **139**, 3747–3755.
98 M. E. Seitz, C. D. Chan, K. L. Opper, T. W. Baughman, K. B. Wagener and K. I. Winey, *J. Am. Chem. Soc.*, 2010, **132**, 8165–8174.
99 T. W. Baughman, C. D. Chan, K. I. Winey and K. B. Wagener, *Macromolecules*, 2007, **40**, 6564–6571.
100 K. L. Opper, D. Markova, M. Klapper, K. Müllen and K. B. Wagener, *Macromolecules*, 2010, **43**, 3690–3698.
101 S. C. Dou, S. H. Zhang, R. J. Klein, J. Runt and R. H. Colby, *Chem. Mater.*, 2006, **18**, 4288–4295.
102 J. P. Gong, *Soft Matter*, 2010, **6**, 2583–2590.
103 S. Suzuki, T. Uneyama and H. Watanabe, *Macromolecules*, 2013, **46**, 3497–3504.
104 S. Suzuki, T. Uneyama, T. Inoue and H. Watanabe, *Macromolecules*, 2012, **45**, 888–898.
105 F. J. Stadler, T. Still, G. Fytas and C. Bailly, *Macromolecules*, 2010, **43**, 7771–7778.
106 G. H. Ling, Y. Y. Wang and R. A. Weiss, *Macromolecules*, 2012, **45**, 481–490.
107 A. Shabbir, Q. Huang, G. P. Baeza, D. Vlassopoulos, Q. Chen, R. H. Colby, N. J. Alvarez and O. Hassager, *J. Rheol.*, 2017, **61**, 1279–1289.
108 A. Shabbir, Q. Huang, Q. Chen, R. H. Colby, N. J. Alvarez and O. Hassager, *Soft Matter*, 2016, **12**, 7606–7612.

109 G. W. Park and G. Ianniruberto, *J. Rheol.*, 2017, **61**, 1293–1305.
110 S. Q. Wang, *Macromolecules*, 1992, **25**, 7003–7010.
111 T. Koga and F. Tanaka, *Macromolecules*, 2010, **43**, 3052–3060.
112 T. A. Witten and M. H. Cohen, *Macromolecules*, 1985, **18**, 1915–1918.
113 R. A. Weiss and H. Y. Zhao, *J. Rheol.*, 2009, **53**, 191–213.
114 T. Schweizer, *J. Rheol.*, 2003, **47**, 1071–1085.
115 A. Bach, H. K. Rasmussen and O. Hassager, *J. Rheol.*, 2003, **47**, 429–441.
116 Y. F. Li, M. Hu, G. B. McKenna, C. J. Dimitriou, G. H. McKinley, R. M. Mick, D. C. Venerus and L. A. Archer, *J. Rheol.*, 2013, **57**, 1411–1428.
117 S. Q. Wang, S. Ravindranath and P. E. Boukany, *Macromolecules*, 2011, **44**, 183–190.